Research Square

Preprints are preliminary reports that have not undergone peer review.
They should not be considered conclusive, used to inform clinical practice,
or referenced by the media as validated information.

Auxin-producing Sphingobium promotes maize growth heterosis under phosphorus deficiency

Peng Yu

pengyu.yu@tum.de

Technicial University of Munich https://orcid.org/0000-0003-1670-8428

Wenxin Zou

Crop Functional Genomics, Institute of Crop Science and Resource Conservation (INRES), University of Bonn, Bonn, Germany

Wei Zhang

Southwest University https://orcid.org/0000-0003-1133-6397

Xiaoming He

Crop Functional Genomics, Institute of Crop Science and Resource Conservation (INRES), University of Bonn, 53113 Bonn, Germany

Xiaofang Huang

Plant Genetics, TUM School of Life Sciences, Technical University of Munich, Freising 85354, Germany https://orcid.org/0009-0005-2260-7238

Shunli Liu

College of Resources and Environment, and Academy of Agricultural Sciences, Southwest University (SWU), Chongqing, People's Republic of China

Danning Wang

Plant Breeding, TUM School of Life Sciences, Technical University of Munich, 85354 Freising, Germany

Ling Gu

Plant Genetics, TUM School of Life Sciences, Technical University of Munich, Freising, Germany

Gabriel Schaaf

Rheinische Friedrich-Wilhelms-University Bonn https://orcid.org/0000-0001-9022-4515

José Ugalde

Rheinische Friedrich-Wilhelms-Universität Bonn

Frank Hochholdinger

University of Bonn

Ming Lang

College of Resources and Environment, and Academy of Agricultural Sciences, Southwest University (SWU), Chongqing, People's Republic of China

Franz Neundorf

Institute of Crop Science, University of Hohenheim, 70599 Stuttgart, Germany

Xinping Chen
Southwest University https://orcid.org/0000-0002-6245-0133

Article

Keywords:

Posted Date: September 8th, 2026

DOI: https://doi.org/10.21203/rs.3.rs-10774468/v1

License: This work is licensed under a Creative Commons Attribution 4.0 International License.
Read Full License

Additional Declarations: There is **NO** Competing Interest.

Auxin-producing *Sphingobium* promotes maize growth heterosis under phosphorus deficiency

Wenxin Zou[1,3,4#], Wei Zhang[1,#], Xiaoming He[1,3,4], Xiaofang Huang[2,3], Shunli Liu[1], Danning Wang[5], Ling Gu[2,3], Gabriel Schaaf[6], José Manuel Ugalde[7], Franz Neundorf[8], Frank Hochholdinger[4], Ming Lang[1,*], Xinping Chen[1,*], Peng Yu[2,3,4,*]

[1] College of Resources and Environment, and Academy of Agricultural Sciences, Southwest University (SWU), Chongqing, People's Republic of China

[2] Plant Genetics, TUM School of Life Sciences, Technical University of Munich, Freising, Germany

[3] Emmy Noether Group Root Functional Biology, Institute of Crop Science and Resource Conservation (INRES), University of Bonn, Bonn, Germany

[4] Crop Functional Genomics, Institute of Crop Science and Resource Conservation (INRES), University of Bonn, Bonn, Germany

[5] Plant Breeding, TUM School of Life Sciences, Technical University of Munich, Freising, Germany

[6] Plant Nutrition, Institute of Crop Science and Resource Conservation (INRES), University of Bonn, 53115 Bonn, Germany

[7] Chemical Signalling, Institute of Crop Science and Resource Conservation (INRES), University of Bonn, 53117 Bonn, Germany

[8] Institute of Crop Science, University of Hohenheim, 70599 Stuttgart, Germany

[#] These authors contributed equally:
Wenxin Zou, Wei Zhang

Correspondence:
pengyu.yu@tum.de
chenxp2017@swu.edu.cn
langming@swu.edu.cn

Abstract

Phosphorus (P) deficiency is a major constraint on crop productivity, yet the microbial functions contributing to heterosis (hybrid vigor, the superior F1 performance versus inbred parents) under P limitation remain largely unknown. Here, we investigated rhizosphere microbiome assembly across 93 maize hybrid-inbred triplets grown under contrasting P conditions. Integrating plant performance, phosphorus accumulation, and the microbial abundance identified *Sphingobium* as a bacterial taxon consistently enriched in hybrid rhizospheres under P deficiency. A hybrid-enriched *Sphingobium* isolate (W6) preferentially promoted hybrid growth under low-P conditions, enhancing lateral root development, phosphorus acquisition, and biomass heterosis. Inhibition of auxin transport by N-1-naphthylphthalamic acid (NPA) abolished the W6-mediated growth promotion, whereas DR5::GUS assays and transcriptomic analyses revealed enhanced auxin responses following W6 inoculation. Genome analysis further identified the indole-3-pyruvate pathway as the predominant route for auxin biosynthesis in W6. Together, our findings demonstrate that a hybrid-enriched rhizobacterial function promoting auxin-dependent root architectural plasticity, rather than phosphorus mobilization alone, contributes to maize heterosis under phosphorus deficiency, providing mechanistic insight into how host–microbiome interactions improve crop adaptation to nutrient-limited environments.

Introduction

Heterosis, or hybrid vigor, has been extensively exploited in modern agriculture because it enhances crop productivity, resource-use efficiency, and environmental adaptability (Springer and Stupar, 2007). Hybrid maize accounts for the majority of global maize production, making heterosis one of the most economically important biological phenomena underpinning modern crop improvement (Baldauf et al., 2018). Although heterosis is classically viewed as a consequence of genetic interactions between parental genomes (Hochholdinger and Yu, 2025), emerging evidence suggests that the rhizosphere microbiome also contributes to hybrid performance (Araujo et al., 2024). Maize hybrids assemble rhizosphere microbial communities that differ significantly from those of their parental inbred lines, suggesting that microbiome composition itself can exhibit heterosis-like patterns (Wagner et al., 2020). Consistent with this, Wagner et al. (2021) demonstrated that maize heterosis is strongly influenced by the belowground microbial environment, as heterotic growth was diminished under sterile conditions but restored by live soil microbiota or a simplified bacterial synthetic community, highlighting the context-dependent contribution of microbial communities to hybrid vigor. Recent evidence further indicates that maize hybrids display attenuated pattern-triggered immunity relative to their parental lines, suggesting that heterosis may partly arise from a rebalancing between growth–defense trade-offs during plant-microbe interactions (Hudson et al., 2026). Similar microbiota heterosis has also been observed in hybrid rice, where a hybrid-associated root bacterial community conferred superior protection against soil-borne fungal pathogens through ROS (reactive oxygen species)- and cell wall-related defense pathways (Zhang et al., 2023). Such immune modulation could favor the recruitment and activity of growth-promoting rhizobacteria, thereby enhancing nutrient acquisition and hybrid performance. Providing the first evidence that a specific microbial taxon contributes to heterosis, He et al. (2025) showed that maize hybrids selectively enrich *Massilia* under nitrogen deficiency, and that its abundance is associated with lateral root development, rhizosheath formation, and enhanced hybrid performance. These findings suggest that hybrid-specific recruitment of beneficial microbiome functions can contribute to nutrient-stress adaptation by modulating root architecture and the root-soil interface. However, the specific microbial traits

that contribute to heterosis and the mechanisms through which they influence hybrid performance remain largely unresolved.

Phosphorus (P) is an essential macronutrient that frequently limits crop productivity because of its low mobility and poor bioavailability in soils (Raymond et al., 2021). Plants adapt to P limitations through coordinated changes in direct phosphate uptake, root system architecture, root exudation and microbe-dependent nutrient acquisition pathways (Zhao et al., 2024). Phosphate-solubilizing and mineralizing microorganisms enhance P availability through the production of organic acids, phosphatases, and other metabolites (Peñuelas et al., 2026), whereas microbial signaling molecules can reshape root system architecture (Verbon and Liberman, 2016) and thereby increase soil exploration. These findings support the emerging concept that heterosis may partly arise from the selective recruitment of microbial functions that complement environmental constraints (Hochholdinger and Yu, 2025). Despite the recognized importance of rhizosphere microorganisms in P cycling, the microbial taxa and functions that contribute to heterosis under P deficiency have not been identified. In particular, it is unclear whether hybrids preferentially enrich microbial taxa that promote root developmental plasticity and phosphorus acquisition, and how such microbial functions interact with host signaling pathways to influence heterosis.

Here, we investigated rhizosphere microbiome assembly in 93 maize hybrid–inbred triplets grown under contrasting phosphorus conditions. We identified *Sphingobium* as a bacterial taxon consistently enriched in hybrid rhizospheres under P deficiency and isolated a high auxin-producing strain, W6. Functional validation demonstrated that W6 preferentially enhanced hybrid performance by stimulating lateral root development and phosphorus acquisition through host auxin signaling. Our findings reveal a microbiome-mediated mechanism underlying heterosis under phosphorus limitation and suggest that hybrid-specific recruitment of growth-promoting microbial functions represents an adaptive strategy for nutrient acquisition in resource-limited environments.

Results

Rhizosphere microbiome heterosis is linked to phosphorus acquisition in maize hybrids

To investigate whether rhizosphere microorganisms contribute to maize adaptation to phosphorus deficiency, we evaluated 93 hybrid-inbred triplets representing three major heterotic groups under low- and high-P conditions (Fig. 1a). As expected, shoot biomass and shoot phosphorus accumulation increased with phosphorus supply, and hybrids consistently outperformed their parental inbred lines under both nutrient regimes (Fig. 1c,d). Mid-parent heterosis (MPH) analysis further showed that biomass heterosis was significantly greater under high-P than low-P conditions, whereas heterosis for phosphorus accumulation was largely maintained across P treatments (Fig. 1e,f).

Amplicon sequencing revealed clear differences in bacterial community composition between rhizosphere and bulk soils as well as between phosphorus treatments (PERMANOVA, $P < 0.001$; Fig. 1b). Moreover, hybrids assembled rhizosphere bacterial communities that differed significantly from those of their parental inbred lines under both low- and high-P conditions (PERMANOVA, $P < 0.001$, Supplementary Fig. 1).

To identify bacterial taxa associated with heterosis, we integrated microbial abundance with plant biomass and phosphorus accumulation. Several dominant genera, including *Sphingobium*, *Nocardioides*, *Glycomyces*, and *Lysobacter*, were significantly enriched in hybrid rhizospheres. Among these, *Sphingobium* was the most abundant hybrid-enriched genus under low-P conditions, whereas *Chitinophaga* predominated under high-P conditions (Fig. 2a). The abundance of *Sphingobium* and *Nocardioides* was positively correlated with both biomass and shoot phosphorus accumulation under low-P conditions (Fig. 2c). Furthermore, the MPH of *Sphingobium* abundance was significantly associated with the MPH of plant biomass and phosphorus accumulation, indicating that microbiome heterosis and plant heterosis are closely linked (Fig. 2b).

Amplicon Sequence Variant (ASV)-level analysis identified five *Sphingobium* and twenty-three *Nocardioides* variants, among which *Sphingobium* ASV13 was the dominant taxon and consistently exhibited strong positive heterosis under both phosphorus regimes (Fig. 2d). These

results identify *Sphingobium* as a candidate hybrid-associated bacterium potentially contributing to maize adaptation to phosphorus deficiency.

Auxin-producing *Sphingobium* preferentially enhances maize heterosis under phosphorus deficiency

To investigate the functional roles of hybrid-associated bacteria, we isolated *Sphingobium* and *Nocardioides* strains from the roots of 4-week-old maize plants grown under low-phosphorus conditions. A total of two *Sphingobium* and eighteen *Nocardioides* isolates were obtained (Fig. 2e). Functional screening revealed that *Nocardioides* W12 exhibited strong organic phosphorus (Po) mineralization activity but no detectable indole-3-acetic acid (IAA) production, whereas *Sphingobium* W6 showed the highest IAA production among all isolates but lacked phosphorus-solubilizing activity (Fig. 2e). The 16S rRNA gene sequence of W6 shared 99.16% identity with the dominant hybrid-enriched ASV13, linking the cultured isolate to the microbiome heterosis analysis.

To evaluate the breeding relevance of these bacterial taxa, we examined their abundance across 93 maize hybrid-inbred triplets. Positive heterosis for both *Sphingobium* and *Nocardioides* abundance was observed across the major heterotic groups under both phosphorus regimes, with particularly strong enrichment in tropical germplasm (Supplementary Fig. 3). Among all combinations, the stiff-stalk line × non-stiff-stalk line combination exhibit excellent hybrid performance in commercial germplasm and is efficient for preliminary screening in breeding (Nelson and Goodman, 2008; Kadoumi et al., 2025). The result showed cross between the stiff-stalk line B73 and the non-stiff-stalk line PHG47 exhibited the highest accumulation of both bacterial taxa and was therefore selected for functional validation.

To distinguish the contributions of microbial auxin production and phosphorus mineralization, four representative strains were selected: *Sphingobium* W6 (high IAA production) and W39 (low IAA production), both lacking phosphorus-solubilizing activity, and *Nocardioides* W12 (high Po mineralization) and W35 (low Po mineralization), both lacking IAA production. Inoculation experiments revealed distinct effects of the two microbial functions on plant performance. Both *Sphingobium* strains significantly increased the biomass of the hybrid,

whereas W6 additionally promoted root development (Fig. 3a,b). In contrast, *Nocardioides* strains preferentially promoted the growth of the maternal inbred line B73, with *Nocardioides* W12 producing the strongest increase in shoot phosphorus accumulation across all genotypes (Fig. 3d). Notably, inoculation with *Nocardioides* largely eliminated the biomass and phosphorus differences between B73 and the hybrid.

We further quantified the effects of bacterial inoculation on heterosis. *Sphingobium* W6 significantly increased biomass heterosis, whereas *Nocardioides* W12 resulted in negative heterosis for both biomass and phosphorus accumulation (Fig. 3c, e). Together, these results demonstrate that auxin-producing *Sphingobium* preferentially promotes hybrid performance under phosphorus deficiency, whereas phosphorus-mineralizing *Nocardioides* enhances phosphorus acquisition but does not reinforce maize growth heterosis.

Sphingobium **and** ***Nocardioides*** **differentially regulate growth and defense programs in maize hybrids**

To investigate the molecular basis underlying the contrasting effects of *Sphingobium* W6 and *Nocardioides* W12 on maize heterosis, we compared root transcriptomes and metabolite profiles following bacterial inoculation. Principal component analysis revealed clear separation among the three inoculation treatments, with *Nocardioides* W12 inducing the largest transcriptional shift and *Sphingobium* W6 also exhibiting a distinct expression profile relative to the mock control (Fig. 4a).

Comparisons between the hybrid and its parental inbred lines identified 621 hybrid-specific differentially expressed genes (DEGs) under *Sphingobium* W6 inoculation and 1,833 under *Nocardioides* W12 inoculation (Supplementary Fig. 4a). Based on dominance analysis, 573 and 1,570 of these genes displayed non-additive expression patterns, respectively (Supplementary Fig. 4b,c). Functional enrichment analysis revealed fundamentally different host responses to the two bacterial taxa. Under *Sphingobium* W6 inoculation, the plant hormone signal transduction pathway was the most significantly enriched category, with auxin-responsive genes representing the dominant component (Fig. 4a, Supplementary Fig. 5). Several auxin signaling genes, including *AFB1*, *IAA21*, and *IAA3*, were significantly downregulated in the

hybrid, whereas *IAA34* and *ARF24* were upregulated (Fig. 4c), indicating extensive reprogramming of the host auxin signaling network.

In contrast, *Nocardioides* W12 primarily activated plant-pathogen interaction pathways, with significant enrichment of genes involved in bacterial recognition, anion channel regulation, and defense responses (Supplementary Figs. 6 and 7). These contrasting transcriptional profiles suggest that W6 and W12 are associated predominantly with hormone/auxin-related and defense-related host responses, respectively.

Metabolomic analysis further supported this distinction. K-means clustering identified metabolite cluster 6 specifically enriched under *Sphingobium* W6 inoculation (Fig. 4d and Supplementary Fig. 8), including elevated mid-parent heterosis for 2-hydroxy-2-methylbutanoic acid and N6-methyladenosine (m^6A). Metabolite profile cluster 9 was enriched following inoculation with *Nocardioides* W12 (Supplementary Fig. 9), including elevated mid-parent heterosis for allelochemicals-terephthalic acid and phthalic acid. These results indicate that *Sphingobium* W6 is associated with metabolic reprogramming linked to growth promotion, whereas *Nocardioides* W12 preferentially induces defense-related responses.

Host auxin signaling mediates the growth-promoting effect of *Sphingobium*

To determine whether the growth-promoting effect of *Sphingobium* W6 depends on host auxin signaling, we performed auxin transport inhibition and DR5::GUS reporter assays. Application of the auxin efflux inhibitor N-1-naphthylphthalamic acid (NPA) markedly suppressed plant growth and root development, resulting in wilted and reddened leaves across all genotypes (Fig. 5a). Under NPA treatment, no significant difference in shoot biomass was observed between the hybrid and its parental inbred lines under either mock or W6 inoculation (Fig. 5b).

In the absence of NPA, all genotypes recovered normal growth, and inoculation with *Sphingobium* W6 significantly increased the shoot biomass of the hybrid relative to the mock treatment (Fig. 5b). Correspondingly, biomass heterosis was not significantly altered by W6 inoculation under NPA treatment, whereas W6 significantly increased biomass MPH in the absence of NPA (Wilcoxon rank-sum test, $P < 0.05$; Fig. 5c). These results indicate that the growth-promoting effect of W6 requires functional auxin transport from the host.

We then quantified root traits including total root length, lateral root number and lateral root density of primary root (Fig. 5d, Supplementary Fig. 10a,b). Under without NPA treatment, W6 inoculation increased lateral root number and density, especially in hybrid, while the total primary root length was lower than that in mock. Under NPA treatment, the root development was suppressed in both of W6 and mock treatment (Fig. 5d). Moreover, W6 significantly increased MPH of lateral root density and lateral root number under without NPA treatment (Wilcoxon rank-sum test, $P < 0.05$; Fig. 5e, Supplementary Fig.10c), while there was no significant difference that root length MPH (Supplementary Fig.10d), suggesting that the W6 play a key role in lateral root development.

To further examine auxin responses, DR5::GUS reporter assays were performed in *Arabidopsis thaliana*. Inoculation with *Sphingobium* W6 enhanced DR5::GUS activity in lateral root tips, whereas control plants showed stronger auxin accumulation in the primary root tip (Fig. 5f, g), suggesting that W6 promotes the redistribution of auxin toward lateral root development. We next sequenced the complete genome of *Sphingobium* W6, which consists of 4,755,549 bp with a GC content of 63.19% (Supplementary Fig. 11). Genome annotation identified several genes involved in indole-3-acetic acid (IAA) biosynthesis, including the tryptophan synthesis genes *trpA* and *trpB*, as well as the indole-3-acetone dehydrogenase gene (*ipdC*) in the indole-3-pyruvate (IPyA) metabolic pathway, indicating that the IPyA pathway is the predominant route for auxin biosynthesis in W6.

Discussion

The contribution of the rhizosphere microbiome to plant heterosis has recently emerged as an important research frontier. Previous studies demonstrated that maize hybrids assemble rhizosphere microbial communities distinct from those of their parental inbred lines and that the expression of heterosis depends, at least in part, on interactions with the soil microbiome (Wagner et al., 2020, 2021). More recently, the hybrid-enriched bacterium *Massilia* was shown to promote heterosis under nitrogen deficiency by stimulating lateral root development (He et al., 2025). Whether analogous microbiome functions contribute to heterosis under phosphorus limitation, however, has remained unknown. By integrating multi-omics profiling across 93 maize hybrid-inbred triplets with functional validation, we demonstrate that microbiome-associated heterosis under phosphorus deficiency extends beyond microbial phosphorus mobilization. Instead, hybrid-enriched microbial functions that promote root architectural plasticity through host auxin signaling are closely associated with enhanced phosphorus acquisition and hybrid performance (Fig. 6).

Hybrid-enriched auxin-producing rhizobacteria promote root architectural plasticity under phosphorus deficiency

Phosphorus deficiency substantially reshapes rhizosphere microbial communities and enriches microorganisms capable of mobilizing insoluble phosphorus through phosphatases, phytases, and organic acid secretion (Pang et al., 2024; Peñuelas et al., 2026; Zhan et al., 2026). Consequently, phosphate-solubilizing microorganisms have long been regarded as the principal microbial mechanism underlying improved phosphorus nutrition. However, phosphorus acquisition depends not only on phosphorus availability but also on the ability of roots to efficiently explore the surrounding soil, a process that is strongly influenced by microbial phytohormones (Liu, 2021; Dini-Andreote et al., 2025). Increasing evidence therefore supports the concept that the rhizosphere microbiome functions as an environmentally responsive extension of host traits, influencing plant adaptation to nutrient stress (He et al., 2024; Dwivedi et al., 2025).

Our results suggest that, in the context of heterosis, microbial stimulation of root architectural plasticity contributes more strongly to hybrid performance than phosphorus

mobilization alone. The hybrid-enriched bacterium *Sphingobium* produced high levels of indole-3-acetic acid (IAA), activated host auxin-responsive pathways, promoted lateral root development, and increased biomass heterosis under phosphorus deficiency. In contrast, the organic phosphorus-mineralizing bacterium *Nocardioides* enhanced phosphorus acquisition but did not increase heterosis, indicating that improved direct microbial P mobilization alone is insufficient to explain superior hybrid growth. Similar auxin-mediated promotion of root architectural remodeling has been reported for *Bacillus amyloliquefaciens* during cluster root formation under phosphorus deficiency (Yang et al., 2025). Moreover, a recent study reported a positive association between *Sphingobium* and maize root total P across three maize developmental stages under different P-fertilization treatments (Jia et al., 2026). Because phosphorus diffusion in soil is inherently slow, continued root proliferation into unexplored soil represents an effective strategy for sustaining nutrient acquisition (Dinh et al., 2023; Fujii, 2024; Wen et al., 2025). Together, these findings indicate that microbial regulation of root architectural plasticity constitutes a major functional mechanism contributing to heterosis under phosphorus limitation.

Importantly, these findings complement recent observations under nitrogen deficiency rather than representing an independent mechanism. Under nitrogen limitation, hybrids preferentially recruit *Massilia*, which promotes lateral root development through flavonoid-mediated interactions (He et al., 2025). Under phosphorus limitation, hybrids instead preferentially enrich auxin-producing *Sphingobium*, which activates host auxin signaling to stimulate lateral root formation. Thus, although different nutrient environments favor distinct microbial functions and signalling mechanisms, both are associated with increased root architectural plasticity that may enhance resource acquisition. This emerging framework suggests that nutrient-specific microbiome functions may provide alternative biological solutions for maintaining hybrid vigor under different nutritional constraints.

Distinct host transcriptional responses elicited by growth-promoting and phosphorus-mineralizing bacteria

Transcriptomic analyses further demonstrated that *Sphingobium* and *Nocardioides* elicited distinct host regulatory responses. *Sphingobium* preferentially activated auxin-responsive and growth-associated pathways, whereas *Nocardioides* induced plant-pathogen interaction

pathways together with defense-associated responses. These contrasting transcriptional profiles suggest that different microbial functions engage distinct host regulatory programs. However, because our study did not directly quantify defense costs or resource allocation, these responses should be interpreted as growth-associated and defense-associated transcriptional states rather than evidence for optimization of the growth-defense balance.

The induction of defense-associated pathways by *Nocardioides* is nevertheless consistent with previous observations that phosphorus deficiency is closely linked to immune regulation. Phosphorus starvation has been shown to remodel the rhizosphere microbiome while simultaneously activating innate immunity (Castrillo et al., 2017), and low-phosphorus conditions promote microbiome–metabolite interactions associated with enhanced disease resistance (Liu et al., 2026). Likewise, the bacterial volatile diacetyl was shown to enhance salicylic acid- and jasmonic acid-associated immune responses under phosphorus deficiency, accompanied by reduced plant growth (Morcillo et al., 2020). Together with our findings, these studies suggest that microbial functions associated with phosphorus mobilization and those associated with growth promotion may trigger fundamentally different host transcriptional programs, potentially contributing to contrasting effects on hybrid performance.

Limitations of current study

Several limitations should be acknowledged. First, although the association between *Sphingobium* abundance and heterosis was identified across 93 maize hybrid–inbred triplets, mechanistic validation was performed using a single representative hybrid combination, and the generality of this mechanism across diverse maize germplasm remains to be established. Second, while NPA inhibition and DR5::GUS assays demonstrated that host auxin signaling is essential for the growth-promoting effect of *Sphingobium*, the molecular mechanisms through which hosts perceive and integrate microbial auxin signals remain unresolved. Finally, our experiments focused on individual bacterial isolates, whereas rhizosphere microorganisms naturally function within complex microbial communities. Future studies integrating synthetic microbial communities, host genetics, and diverse environmental conditions will be necessary to determine how microbiome assembly contributes to heterosis across nutrient environments.

Together, our findings support a model in which microbiome-associated heterosis under phosphorus deficiency is driven by nutrient-specific microbial functions that enhance root

architectural plasticity. Hybrids preferentially enrich the auxin-producing bacterium *Sphingobium*, which activates host auxin signaling to stimulate lateral root development, thereby improving phosphorus acquisition and biomass heterosis. In contrast, the phosphorus-mineralizing bacterium *Nocardioides* primarily elicited defense-associated transcriptional responses without enhancing heterosis. Together with previous evidence that *Massilia* promotes heterosis under nitrogen deficiency, our study suggests a unifying framework in which distinct nutrient environments recruit different microbial functions, yet these functions converge on a common developmental outcome—enhanced root architectural plasticity that sustains hybrid vigor under nutrient stress. This framework extends the concept of microbiome-dependent heterosis beyond microbial taxonomy and highlights functional microbiome traits as promising targets for breeding crops with improved nutrient-use efficiency.

Methods

Experimental Design, Treatments, and Maize Materials

The experiment was conducted in a greenhouse under controlled environmental conditions with a 14-h photoperiod, a light intensity of 6,000-10,000 lux, and mean day/night temperatures of 21.5°C and 17.1°C, respectively. A completely randomized block design was employed with four biological replicates, each established as an independent experimental batch at one-week intervals. In each batch, six unplanted pots were maintained as bulk soil (BS) controls.

The soil was collected from the research station in Heßberg, Germany (50°25′ N, 10°46′ E), soil texture was sandy loam. The initial soil available phosphorus concentration was 19 mg kg^{-1}. Soil available phosphorus was determined using the CAL (calcium-acetate-lactate) method (VDLUFA, 1991). Briefly, 5 g soil samples were extracted with 100 ml CAL solution (0.05 M calcium acetate, -lactate acid, pH 4.1) and the P concentration in the filtrate was measured colorimetrically. The initial soil pH was 6.8, measured in 0.01 M $CaCl_2$ at a soil-to-solution ratio of 1:2.5 (w/v) (VDLUFA, 1991), other soil characteristics were described in (Herrmann et al., 2026). The soil was air-dried, passed through a 5-mm sieve, and thoroughly mixed with washed sand at a 1:1 (v/v) ratio. Each pot (7 × 7 × 19 cm; 750 g substrate) was filled with the soil-sand mixture. Based on preliminary experiments and soil nutrient analyses, two phosphorus treatments were established: a low-phosphorus treatment (Low-P), supplemented with 20 mg P kg^{-1} soil, and a high-phosphorus treatment (High-P), supplemented with 200 mg P kg^{-1} soil, both applied as KH_2PO_4. To ensure that phosphorus was the only limiting nutrient, all pots received the following basal nutrients (mg kg^{-1} soil): 200 N (as $Ca(NO_3)_2 \cdot 4H_2O$), 150 K (as K_2SO_4), 4.3 Mg (as $MgSO_4 \cdot 7H_2O$), 8 Fe (as EDTA-FeNa) and 8 Zn (as $ZnSO_4 \cdot 7H_2O$) and 8 Mn (as $MnSO_4 \cdot H_2O$).

The maize panel comprised 93 elite inbred lines, the reference inbred line B73, and 93 corresponding hybrids generated using B73 as the common maternal parent. These materials were selected from an initial population of approximately 300 hybrid combinations to capture broad genetic diversity and a wide range of heterosis levels. Selection criteria included: (i) high phenotypic reproducibility for shoot biomass, with a standard error of less than 0.26 across replicates; (ii) representation of a broad spectrum of mid-parent heterosis (MPH) for shoot biomass; and (iii) inclusion of paternal inbred lines from diverse breeding programs representing the major maize heterotic groups. The final panel consisted of 31 non-stiff stalk, 30 stiff stalk, and 32 tropical inbred lines.

In total, 1,567 samples were collected, including 1,519 rhizosphere samples and 48 bulk soil controls. Among the rhizosphere samples, 743 were obtained under Low-P conditions and 776

under High-P conditions. Bulk soil controls comprised 24 samples from each phosphorus treatment.

Maize Seed Surface Sterilization and Germination

Maize seeds were surface sterilized prior to all experiments to eliminate epiphytic microorganisms as previously described (He et al., 2025). Briefly, seeds were rinsed with sterile deionized water, immersed in 70% (v/v) ethanol for 2 min, and subsequently disinfected in 15 ml sodium hypochlorite solution (12–13% v/v stock solution) containing 1 ml Tween 20. After sterilization, seeds were rinsed three times with sterile deionized water to remove residual disinfectants.

Surface-sterilized seeds were germinated for 3 days using the paper-roll method (Anchor Paper, Saint Paul, MN, USA) as previously described (Hetz et al., 1996). Uniform seedlings were subsequently selected for all experiments.

Rhizosphere Soil Collection and Extraction

Rhizosphere samples were collected from 4-week-old maize plants. After gently shaking the root systems to remove loosely attached bulk soil, the first whorl of crown roots together with tightly adhering rhizosphere soil was excised and transferred into sterile centrifuge tubes. Samples were immediately transported on dry ice and stored at -80 °C until processing.

Rhizosphere soil was extracted from the root segments as previously described (He et al., 2024). Briefly, samples were thawed on ice and incubated in 20 mL sterile phosphate-buffered saline (PBS, pH 7.0) containing 0.02% (v/v) Silwet L-77 (Sigma) with gentle agitation (35 rpm.) for 20 min. The roots were then transferred to fresh extraction buffer, and the procedure was repeated once. The two wash fractions were pooled and centrifuged twice at 4,000 × g for 20 min at 16 °C. The resulting pellet was resuspended in 300 µL sterile water, transferred to a 1-mL lysing matrix tube, snap-frozen in liquid nitrogen, and stored at -80 °C until DNA extraction.

Shoot Biomass and Phosphorus Determination

At harvest, the entire shoot was collected, and shoot dry biomass was determined after oven drying. Dried shoot tissues were ground to a fine powder, and 0.2 g of each sample was digested with 5 mL HNO_3 using a microwave digestion system (Mars 6, CEM Corporation). Phosphorus concentration in the digested solution was quantified using the molybdenum blue colorimetric method (molybdenum-antimony-ascorbic acid assay) with a microplate reader (Infinite M200 Pro, Tecan). P concentration in the digest was converted to shoot-tissue P concentration using the digested sample mass, final digest volume and dilution factor. Shoot phosphorus accumulation was calculated from the product of shoot dry biomass and phosphorus

concentration.

DNA Extraction and Amplicon Sequencing

Total genomic DNA was extracted from frozen rhizosphere samples using the DNeasy PowerSoil DNA Isolation Kit (MoBio Laboratories, USA) according to the manufacturer's instructions. DNA quantity and quality were assessed using a Qubit 2.0 Fluorometer (Thermo Fisher Scientific) and agarose gel electrophoresis.

Bacterial community composition was characterized via amplicon sequencing of the 16S rRNA gene V4 region. A two-step PCR strategy was employed for library construction. In the first PCR, total genomic DNA was amplified using the primer pair 515F (5′-GTGYCAGCMGCCGCGGTAA-3′) and 806R2 (5′-GGACTACNVGGGTWTCTAAT-3′) under the following conditions: initial denaturation at 95 °C for 5 min, followed by 20 cycles of 95 °C for 30 s, 55 °C for 30 s, and 72 °C for 30 s, with a final extension at 72 °C for 10 min. The resulting amplicons were purified using magnetic beads to remove residual primers and enzymes, yielding products flanked by partial adapter sequences. In the second PCR, the purified amplicons were amplified with primers carrying the full-length Illumina adapters (including P5/P7 sequences, index tags, and Read1/Read2 binding sites), thereby incorporating complete adapters to generate the final sequencing library. Library quality was assessed with a Qubit 2.0 Fluorometer and an Agilent 2100 Bioanalyzer, and sequencing was performed on an Illumina NovaSeq 6000 platform in 250-bp paired-end mode.

Raw sequence data were processed using a standard amplicon analysis pipeline, including quality filtering, chimera removal, and amplicon sequence variant (ASV) inference, followed by taxonomic assignment against the SILVA reference database.

Bioinformatic Processing of Amplicon Sequencing Data

Raw paired-end 16S rRNA gene sequences were demultiplexed according to sample-specific barcodes, and barcode and primer sequences were removed prior to analysis. Paired-end reads were merged using FLASH (v1.2.7), and subsequent processing was performed in QIIME 2 (v2020.6).

Raw paired-end reads were first processed using Trimmomatic v0.33, and a sliding window of 50 bp with an average quality threshold of 20 (SLIDINGWINDOW:50:20). Primer sequences were removed using Cutadapt 1.9.1 with the following parameters: a maximum error rate of 0.2 a minimum overlap of 15 bp between read and primer, discarding reads without primer, and retaining only trimmed reads of at least 100 bp. Denoising andASV inference were conducted using the DADA2 plugin implemented in QIIME2 with default parameters. Forward and reverse reads were truncated at 250 bp, and chimeric sequences were identified and removed

using the consensus method. Taxonomic classification was performed using the q2-feature-classifier plugin with a naïve Bayes classifier trained on the SILVA 138 database clustered at 99% sequence identity. A total of 90.18 million reads were obtained, with an average of 57547.78 reads per sample.

ASVs assigned to chloroplasts or mitochondria were removed prior to downstream analyses. The resulting ASV table was imported into R (v4.3.1) for further processing, where ASVs represented by fewer than 10 reads in fewer than two samples were excluded to reduce the influence of spurious low-abundance features. The filtered ASV table was used for all subsequent diversity analyses, differential abundance testing, and data visualization.

Statistical Analysis of Microbial Communities

For microbiome analyses, ASVs with a relative abundance ≤ 0.1% in ≤ 1% of samples and samples containing fewer than 1,000 sequencing reads were excluded. The ASV count table was normalized using the variance stabilizing transformation (VST) implemented in the DESeq2 package (v1.48.1), and batch effects associated with biological replicates were removed using the removeBatchEffect function in the limma package (v3.64.3). Bray-Curtis dissimilarities were calculated from the batch-corrected abundance matrix.

Microbial community composition was evaluated by principal coordinate analysis (PCoA), and differences in β-diversity were tested by permutational multivariate analysis of variance (PERMANOVA) using the adonis2 function in the vegan package (v2.7-1), with genotype and phosphorus treatment as fixed factors and biological replicate as a stratification variable.

Differential abundance analyses were performed at the genus level using two-sided Wilcoxon rank-sum tests, and *P* values were adjusted for multiple comparisons using the Benjamini-Hochberg false discovery rate (FDR) method. Associations between microbial abundance and plant phenotypes were evaluated using Spearman's rank correlation. Correlation matrices and heatmaps were generated using the pheatmap package (v1.0.13), and graphical visualizations were produced with ggplot2 (v4.0.0) in R.

A neighbor-joining phylogenetic tree was constructed using MEGA software, and the distribution of ASV relative abundances was visualized with Interactive Tree of Life (iTOL v7.5.1).

Unless otherwise stated, all statistical analyses were performed in R (v4.3.1), and differences were considered statistically significant at $P < 0.05$.

Calculation of Mid-parent Heterosis

Mid-parent heterosis (MPH) was used to quantify hybrid vigor and was calculated as the relative deviation of the hybrid phenotype from the mean value of its two parental inbred lines:

$$MPH = [F_1 - (P_1 + P_2)/2] / [(P_1 + P_2)/2]$$

where F_1 is the trait value of the hybrid, P_1 is the value of the maternal inbred line (B73), and P_2 is the value of the corresponding paternal inbred line.

MPH was calculated for plant phenotypic traits, including shoot biomass and phosphorus accumulation, as well as for the relative abundance of individual rhizosphere microbial taxa. Positive MPH values indicate that the hybrid exceeded the parental mean, whereas negative values indicate performance below the mid-parent value. For microbial traits, the mid-parent value (MPV) was derived by averaging the two parental mean relative abundances. Subsequently, for each biological replicate of the corresponding hybrid, MPH was computed using this fixed MPV.

Isolation and Functional Characterization of Bacterial Strains

Bacterial strains were isolated from the rhizosphere of maize plants grown under low-phosphorus (Low P) conditions using a high-throughput cultivation pipeline as previously described (14). Briefly, root segments with tightly adhering rhizosphere soil were collected from 4-week-old maize plants, and approximately 0.1 g of pooled material was used for bacterial isolation and parallel 16S rRNA amplicon sequencing. Candidate strains corresponding to hybrid-enriched ASVs were identified by matching 16S rRNA gene sequences. In total, two *Sphingobium* isolates and eighteen *Nocardioides* isolates were recovered.

Bacterial strains were routinely cultured on half-strength tryptic soy broth (1/2 TSB) medium at 28 °C with shaking at 220 rpm for 3 days and adjusted to an optical density of OD600 = 0.1 before functional assays. Plant growth-promoting traits associated with phosphorus acquisition were evaluated, including inorganic phosphate solubilization, organic phosphorus mineralization, and indole-3-acetic acid (IAA) production. Three biological replicates were used for each functional assay. Inorganic phosphate-solubilizing activity and organic phosphorus-mineralizing activity were assessed on Pikovskaya's agar and Menkina's agar

media, respectively. Plates were incubated at 28 °C for 7 days, and the ratios of the transparent halo diameter (D) to the colony diameter (d) were recorded as indicators of phosphorus-mobilizing capacity.

IAA production was quantified using the Salkowski colorimetric assay. Briefly, bacterial cultures were grown in 1/2 TSB medium supplemented with 0.1% (w/v) L-tryptophan for 3 days at 28 °C. Culture supernatants were collected by centrifugation, mixed with an equal volume of Salkowski reagent, and incubated in the dark for 30 min. Absorbance was measured at 530 nm, and IAA concentrations were determined using a standard curve generated with authentic IAA.

Bacterial Inoculation Experiment

To validate the microbial mechanisms underlying maize heterosis under phosphorus deficiency, bacterial inoculation experiments were performed using representative isolates with contrasting functional traits. Two *Sphingobium* strains differing in indole-3-acetic acid (IAA) production but lacking detectable phosphorus-solubilizing activity, and two *Nocardioides* strains differing in organic phosphorus mineralization capacity but lacking IAA production, were selected for functional validation. A mock inoculation with sterile PBS served as the control treatment.

The maize triplet consisting of the maternal inbred line B73, the paternal inbred line PHG47, and their corresponding hybrid (B73 × PHG47), which exhibited high mid-parent heterosis (MPH) for both *Sphingobium* and *Nocardioides* abundance, was used for inoculation assays. Four biological replicates were included for each treatment.

Bacterial strains were cultured in half-strength tryptic soy broth (1/2 TSB) for 3-5 days, harvested by centrifugation, washed, and resuspended in sterile 1× PBS to a final concentration of OD_{600} = 0.02. Surface-sterilized maize seeds were germinated for 3 days, and uniformly developed seedlings with primary roots of approximately 2 cm were immersed in the bacterial suspensions for 3 h with gentle shaking (Yu et al., 2021). Control seedlings were treated with sterile PBS. After inoculation, seedlings were transplanted into pots containing low-phosphorus soil and cultivated under controlled growth chamber conditions (16 h light/8 h dark, 26/18 °C day/night temperature, and 70% relative humidity). No further bacterial suspension was supplemented thereafter.

Plants were irrigated with sterile water throughout the experiment, with watering volumes adjusted according to pot weight. Pots were arranged in a completely randomized design, and tray positions were rotated weekly to minimize positional effects.

RNA Extraction and Transcriptome Sequencing

Total RNA was extracted from the first whorl of separate crown root tissues using Aidlab RN40 Reagent (Aidlab Biotechnologies, China) according to the manufacturer's instructions. RNA concentration and purity were determined using a NanoDrop 2000 spectrophotometer (Thermo Fisher Scientific), and RNA integrity was assessed using a LabChip GX system (PerkinElmer).

Sequencing libraries were prepared using the Hieff NGS Ultima Dual-mode mRNA Library Prep Kit for Illumina (Yeasen, China) together with the MGIEasy Universal Library Conversion Kit (MGI, China) following the manufacturers' protocols. Poly(A)+ mRNA was enriched using oligo(dT)-coupled magnetic beads and used for cDNA library construction. Library quality and concentration were evaluated using a QSep-400 fragment analyzer (BiOptic) and a Qubit 3.0 fluorometer (Thermo Fisher Scientific).

Qualified libraries were sequenced on the DNBSEQ-T7 platform (MGI, Shenzhen, China) to generate 150-bp paired-end reads (PE150). Library preparation and sequencing were performed by Biomarker Technologies (Beijing, China). 4 biological replicates are included.

RNA-seq Data Processing

Raw reads were filtered to remove adapter sequences and low-quality reads. Clean reads were aligned to the maize B73 reference genome (AGPv5) using HISAT2 (v2.2.1). Gene expression levels were quantified with featureCounts, normalized as Fragments Per Kilobase of transcript per Million mapped reads (FPKM) values. Principal component analysis (PCA) was performed on log2(FPKM+1)-transformed expression values using the prcomp function in R, and statistical significance was assessed by PERMANOVA (adonis2) with Euclidean distance. Genes with an adjusted P value < 0.05 and $|\log2(\text{fold change})| > 1$ were considered differentially expressed and differential expression analysis was performed using DESeq2. To investigate the biological functions of the differentially involved pathways, Gene Ontology (GO) term and Kyoto Encyclopedia of Genes and Genomes (KEGG) pathway enrichment analyses were performed.

Characterization of Dominance Patterns and Identification of Non-additively Expressed Genes

To characterize the inheritance patterns of gene expression in the hybrid, the dominance index ($D/|A|$) was calculated for differentially expressed genes (DEGs) following established methods (Liu et al., 2020). The dominance effect (D) and additive effect (A) were defined as: $D = F_1 - (P_1 + P_2)/2$, and the additive effect (A) as $A = (P_1 - P_2)/2$. Based on the value of $D/|A|$, gene expression patterns in the hybrid were classified into seven distinct categories according to previously defined criteria (Ye et al., 2023, Chen et al., 2025): additive (A: $D/|A| < 0.2$), up-regulated partial-dominance (PD: $0.2 \leq D/|A| < 0.8$), down-regulated partial-dominance (PD-:

-0.8 ≤ D/|A| < -0.2), up-regulated full-dominance (FD: 0.8 ≤ D/|A| < 1.2), down-regulated full-dominance (FD-: -1.2 ≤ D/|A| < -0.8), up-regulated overdominance (OD: D/|A| ≥ 1.2) and down-regulated overdominance (OD: D/|A| ≤ -1.2).

To identify non-additively expressed genes (NAE-DEGs), DEGs shared between the comparisons B73 versus hybrid (B73 × PHG47) and PHG47 versus hybrid were first identified by Venn analysis. Genes that were differentially expressed between the hybrid and both parental lines were regarded as hybrid-specific DEGs. Among these genes, those exhibiting partial dominance, complete dominance, or overdominance expression patterns were classified as NAE-DEGs and were subsequently used for downstream functional enrichment and pathway analyses.

Root Exudate Collection and Metabolite Extraction

To investigate whether bacterial inoculation alters root exudation patterns, root exudates were collected from B73, PHG47, and their hybrid (B73 × PHG47) after 4 weeks of growth under different bacterial inoculation treatments. For each genotype and treatment, 4 biological replicates are included. Root exudates were recovered using a modified hydroponic collection system based on Williams et al. (2021).

Briefly, a recovery solution was prepared by suspending 200 g of field soil in 1 L of Milli-Q water, followed by sedimentation and filtration through a 0.2-mm mesh. Plants were carefully removed from the pots, and roots were gently washed with distilled water to remove adhering soil particles. The cleaned root systems were immersed in the recovery solution and maintained under the same environmental conditions as plant growth with continuous aeration for 24 h to allow physiological recovery from transplanting stress.

After the recovery period, root systems were transferred aseptically to sterile glass jars containing 100 mL distilled water and incubated for 2 h with gentle shaking (60 rpm) to collect root exudates. To minimize microbial degradation, exudate solutions were maintained on ice during processing. The collected solutions were filtered through 0.22-μm syringe filters under sterile conditions to remove microorganisms and particulate matter.

Filtered exudates were immediately frozen at -80 °C, lyophilized, and stored at -80 °C until metabolomic analysis.

Metabolite Profiling and Data Analysis

Freeze-dried root exudate samples (50 mg) were extracted with methanol/acetonitrile/water (2:2:1, v/v/v), homogenized, sonicated in an ice-water bath, and incubated at -20 °C to facilitate metabolite extraction. 4 biological replicates are included. After centrifugation, the supernatants

were collected, vacuum dried, and reconstituted in acetonitrile/water (1:1, v/v). Quality control (QC) samples were prepared by pooling equal aliquots from all biological samples and were injected every 10 samples.

Wide-Targeted Metabolomics was performed using an Ultra-Performance Liquid Chromatography system (Waters Acquity UPLC I-Class PLUS) coupled to an AB Sciex QTRAP 6500+ mass spectrometer. Chromatographic separation was achieved on an Acquity UPLC HSS T3 column, and metabolites were detected in both positive and negative electrospray ionization modes using multiple reaction monitoring (MRM).

Raw data were processed by peak integration and normalization, and metabolite annotation was performed by comparing retention times and MS/MS spectra against the BMKGENE metabolite database. During data processing, isotope peaks, adduct-related signals (including K^+, Na^+, and NH_4^+), as well as duplicate signals originating from in-source fragmentation of larger metabolites, were removed to minimize potential interference. Differential metabolites were clustered by their abundance variation patterns using the K-means algorithm. Data were Z-score normalized prior to analysis, with Euclidean distance as the similarity metric. The optimal cluster number (k) was determined by the elbow criterion. After iterative assignment and centroid updating until convergence, metabolites with similar trends were grouped together, and each cluster's representative pattern was visualized by its centroid profile.

Auxin Transport Inhibition Assay

To determine whether the growth-promoting effects of *Sphingobium* W6 depend on host auxin transport, an auxin efflux inhibition experiment was conducted using the maize triplet comprising B73, PHG47, and their hybrid (B73 × PHG47). The auxin transport inhibitor 1-naphthylphthalamic acid (NPA) was applied at a final concentration of 10 μM (Xu et al., 2023; Xu et al., 2025), while sterile water served as the control treatment.

The experiment was performed using a unplanted, phosphorus-deficiency fluvo-aquic soil collected from Hebei Province, China (36.9°N, 115.0°E). The soil texture was clay loam, the soil available phosphorus was determined using the Olsen method (Olsen, 1954). Briefly, soil samples were extracted with 0.5 M $NaHCO_3$ (pH 8.5) and quantified by colorimetry. The fluvo-aquic soil available phosphorus concentration was 8.66 mg kg^{-1}, and soil pH was 8.3. The soil was sterilized by gamma irradiation (25 kGy) and supplemented with the same nutrient solution described above. Each pot (12 × 8 × 16 cm) contained 1 kg of sterilized soil.

Consistent with the bacterial inoculation experiment, Surface-sterilized maize seeds were germinated for 3 days and inoculated with *Sphingobium* W6 for 3 h before transplantation. NPA and control solutions were applied at planting. 5 mL second bacterial suspension (OD_{600} = 0.02) application was carried out at 10 days after sowing for the inoculated treatments. Plants were grown under controlled conditions and harvested 3 weeks after transplantation for phenotypic analyses. The entire root system was carefully excised and rinsed with water. Root traits, including primary root length, total lateral root number, and lateral root density, were assessed. Lateral root density was determined for the primary roots by manually counting the number of emerged lateral roots per unit length (cm) of the primary root. 5 biological replicates in each genotype and treatment.

DR5::GUS Assay for Auxin Signaling Activation

To determine whether *Sphingobium* sp. W6 activates host auxin signaling, the auxin-responsive reporter line DR5::GUS of *Arabidopsis thaliana* (Columbia-0) was used (Yu et al., 2021). Bacterial cultures were grown in half-strength tryptic soy broth (1/2 TSB) for 3 days, harvested by centrifugation, washed, and resuspended in sterile 1× PBS to a final concentration of OD_{600} = 0.01.

After surface sterilization and 48 h stratification, DR5::GUS seeds were germinated on half-strength Murashige and Skoog (1/2 MS) medium. The roots of 4-day-old seedlings were inoculated with 8 μL of bacterial suspension, whereas sterile PBS was used as the control treatment. Histochemical GUS staining was performed 3 days after inoculation following standard procedures. Stained seedlings were examined and imaged using a Leica light microscope. GUS expression of each primary root or lateral root was relative quantified by measuring the percentage of stained area using ImageJ software.

The experiment included three independent biological replicates, with five seedlings analyzed per replicate.

Whole-genome Sequencing of *Sphingobium* W6

High-molecular-weight genomic DNA was extracted from *Sphingobium* W6 using a genomic

DNA purification kit following the manufacturer's instructions. DNA quantity and quality were evaluated using a NanoDrop spectrophotometer, a Qubit fluorometer, and agarose gel electrophoresis.

A long-read sequencing library was constructed using the PacBio SMRTbell library preparation workflow. Briefly, genomic DNA was fragmented, end repaired, ligated to SMRTbell adapters, size selected, and purified according to the manufacturer's protocols. The final library was sequenced on the PacBio Revio Single Molecule Real-Time (SMRT) platform (Pacific Biosciences, USA).

Raw sequencing reads were assembled de novo to generate the complete genome sequence of *Sphingobium* W6. Genome annotation was performed using standard bacterial genome annotation pipelines, and genes associated with indole-3-acetic acid (IAA) biosynthesis were identified based on functional annotation against public databases.

Genome Assembly and Functional Annotation

Genome assembly was performed using Flye v2.8.2 with the high-fidelity (HiFi) reads. The assembled sequence was circularized using Circlator v1.5.5 to resolve high-quality contig ends, and further polished with Illumina short-read data using Pilon v1.22 to improve assembly accuracy. Genome completeness was evaluated using BUSCO.

Gene prediction and genome annotation were performed using standard bacterial genome annotation pipelines, and functional assignments were obtained by comparison with the KEGG, COG, Swiss-Prot, and NR databases. Putative indole-3-acetic acid (IAA) biosynthetic genes were identified based on KEGG pathway annotation and manual curation of tryptophan metabolism-related genes, allowing reconstruction of the auxin biosynthetic pathways in *Sphingobium* W6. The genome assembly and gene annotation were visualized as a Circos diagram using Circos v0.66.

Statistical Analyses

Phenotypic data, including shoot biomass, phosphorus accumulation, and their corresponding mid-parent heterosis (MPH) values, were visualized using Origin 2022. Pairwise comparisons were performed using two-sided Wilcoxon rank-sum tests, whereas comparisons among

684 multiple groups were analyzed by one-way analysis of variance (ANOVA) followed by
685 Duncan's multiple range test.
686

Acknowledgments

We thank Prof. Dr. Corinna Dawid and Andreas Daschner (Food Chemistry and Molecular Sensory Science, Technical University of Munich, Germany) for helping with freeze-drying of root exudate samples. We thank Nur Gömec (Plant Nutrition, Institute of Crop Science and Resource Conservation, University of Bonn, Germany) for valuable assistance with the determination of shoot phosphorus concentrations. This research was supported by the Deutsche Forschungsgemeinschaft (DFG) through the Emmy Noether Programme 444755415 and the DFG Priority Program (SPP2089) 'Rhizosphere Spatiotemporal Organisation - A Key to Rhizosphere Functions' grant 403671039 to P.Y., and DFG project 552843484 (YU 272/5-1 to P.Y. and SCHA 1274/7-1 to G.S., and the National Key Research and Development Program of China (2023YFD1900600), National Natural Science Foundation (No.32272800) to M.L., China Scholarship Council (No. 202306990056 to M.L, No. 202206990029 to W.Z). The National Maize Production System in China (CARS-02) to X.C.

Competing interests

The authors declare no competing interests.

Data availability

Raw 16S rRNA gene amplicon sequencing data generated in this study have been deposited in the National Center for Biotechnology Information (NCBI) Sequence Read Archive (SRA) under BioProject accession number PRJNA1470288. RNA-sequencing data from the bacterial inoculation experiments have been deposited in the NCBI SRA under BioProject accession number PRJNA1473064. The complete genome sequence of *Sphingobium* W6 has been deposited in GenBank under accession number PRJNA1482320. Source data underlying all figures and supplementary figures are provided with this paper.

Code availability

The code for this project can be found at: https://github.com/zouwx060/project1.

References

Araujo, A.S.F., Sharma, S., Pinheiro, J.B., Lopes, A.C.D.A., 2024. Beyond plant genetics: microbiome-enhancing heterosis in plants. Trends Plant Sci 29 (12), 1292-1294. https://coi.org/10.1016/j.tplants.2024.07.015.

Baldauf, J.A., Hochholdinger, F., 2023. Molecular dissection of heterosis in cereal roots and their rhizosphere. Theor Appl Genet 136 (8), 173. https://coi.org/10.1007/s00122-023-04419-6.

Castrillo, G., Teixeira, P.J.P.L., Paredes, S.H., Law, T.F., de Lorenzo, L., Feltcher, M.E., Finkel, O.M., Breakfield, N.W., Mieczkowski, P., Jones, C.D., Paz-Ares, J., Dangl, J.L., 2017. Root microbiota drive direct integration of phosphate stress and immunity. Nature 543 (7646), 513-518. https://coi.org/10.1038/nature21417.

Chen, J., Zhang, M., Zhang, Q., Hou, X., Jia, D., Gu, Y., Wan, H., Zhao, H., Wen, J., Yi, B., Fu, T., Shen, J., Zhao, L., 2025. Hybrid epigenome unveils parental genetic divergence shaping salt-tolerant heterosis in brassica napus. New Phytol 248 (3), 1475-1490. https://coi.org/10.1111/nph.70532.

Dinh, L.T., Ueda, Y., Gonzalez, D., Tanaka, J.P., Takanashi, H., Wissuwa, M., 2023. Novel qtl for lateral root density and length improve phosphorus uptake in rice (oryza sativa l.). Rice (N Y) 16 (1), 37. https://coi.org/10.1186/s12284-023-00654-z.

Dini Andreote, F., Wells, D.M., Atkinson, J.A., Atkinson, B.S., Finkel, O.M., Castrillo, G., 2025. Microbial drivers of root plasticity. New Phytol 248 (1), 52-67. https://coi.org/10.1111/nph.70371.

Dwivedi, S.L., Vetukuri, R.R., Kelbessa, B.G., Gepts, P., Heslop-Harrison, P., Araujo, A.S.F., Sharma, S., Ortiz, R., 2025. Exploitation of rhizosphere microbiome biodiversity in plant breeding. Trends Plant Sci. https://coi.org/10.1016/j.tplants.2025.04.004.

Fujii, K., 2024. Plant strategy of root system architecture and exudates for acquiring soil nutrients. Ecol Res 39 (5), 623-633. https://coi.org/10.1111/1440-1703.12477.

He, X., Gu, L., Wang, D., Baer, M., Schaaf, G., Apostolakis, A., Meijide, A., Chen, X., Hochholdinger, F., Yu, P., 2025. Rhizosheath inhabiting massilia are linked to heterosis in roots of maize. Nat Commun 16 (1), 10777. https://coi.org/10.1038/s41467-025-65829-2.

He, X., Wang, D., Jiang, Y., Li, M., Delgado-Baquerizo, M., Mclaughlin, C., Marcon, C., Guo, L., Baer, M., Moya, Y.A.T., von Wirén, N., Deichmann, M., Schaaf, G., Piepho, H., Yang, Z., Yang, J., Yim, B., Smalla, K., Goormachtig, S., de Vries, F.T., Hüging, H., Baer, M., Sawers, R.J.H., Reif, J.C., Hochholdinger, F., Chen, X., Yu, P., 2024. Heritable microbiome variation is correlated with source environment in locally adapted maize varieties. Nat Plants 10 (4), 598-617. https://coi.org/10.1038/s41477-024-01654-7.

Hetz, W., Hochholdinger, F., Schwall, M., Feix, G., 1996. Isolation and characterization ofrtcs, a maize mutant deficient in the formation of nodal roots. Plant J 10 (5), 845-857. https://coi.org/10.1046/j.1365-313X.1996.10050845.x.

Herrmann, M.N., Ginter, M., Neundorf, F., Wanke, D., Müller, T., Neumann, G., Bradáčová, K., 2026. Do short - term legume–maize sequences outperform maize monoculture regarding biomass production and p use efficiency under p - restricted conditions? J Plant Nutr Soil Sci (1999) 189 (2), 276-286. https://coi.org/10.1002/jpln.70060.

Hochholdinger, F., Yu, P., 2025. Molecular concepts to explain heterosis in crops. Trends Plant Sci 30 (1), 95-104. https://coi.org/10.1016/j.tplants.2024.07.018.

Hudson, A.I., Wagner, M.R., Balint-Kurti, P.J., 2026. Maize hybrids exhibit reduction in an elicitor-triggered defense response compared with their inbred parents. Mol Plant Microbe In 8-25. https://coi.org/10.1094/MPMI-08-25-0100-SC.

Jia, Z., Zhu, L.F., Wang, L., Zhang, J., Liu, S., Tian, F., Yi, Y., Wang, J., Tang, J., Gong, J., 2026. Phosphorus application, nutrient absorption, and endophytic root bacterial communities in maize grown in phosphorus-deficient rocky arid soils, china. Sci Rep 16 (1), 17237. https://coi.org/10.1038/s41598-026-47922-8.

Kadoumi, R., Heslot, N., Henriot, F., Murigneux, A., Berton, M., Moreau, L., Charcosset, A., 2025. Evolution of population structure in a commercial european hybrid dent maize breeding program and consequences on genetic diversity. Theor Appl Genet 138 (9), 233. https://coi.org/10.1007/s00122-025-05008-5.Liu, D., 2021. Root developmental responses to phosphorus nutrition. J Integr Plant Biol 63 (6), 1065-1090. https://coi.org/10.1111/jipb.13090.

Liu, H., Wang, Q., Chen, M., Ding, Y., Yang, X., Liu, J., Li, X., Zhou, C., Tian, Q., Lu, Y., Fan, D., Shi, J., Zhang, L., Kang, C., Sun, M., Li, F., Wu, Y., Zhang, Y., Liu, B., Zhao, X.Y., Feng, Q., Yang, J., Han, B., Lai, J., Zhang, X.S., Huang, X., 2020. Genome-wide identification and analysis of heterotic loci in three maize hybrids. Plant Biotechnol J 18 (1), 185-194. https://coi.org/10.1111/pbi.13186.

Liu, X., Yang, S., Xie, P., Niu, G., Shen, Q., Yuan, J., 2026. Phosphorus availability drives rhizosphere metabolite-microbial community interactions to modulate cucumber susceptibility to fusarium wilt. Microbiome 14 (1), 132. https://coi.org/10.1186/s40168-026-02381-1.

Morcillo, R.J.L., Singh, S.K., He, D., Vílchez, J.I., Kaushal, R., Wang, W., Huang, W., Paré, P.W., Zhang, H., 2020. Bacteria-derived diacetyl enhances arabidopsis phosphate starvation responses partially through the della-dependent gibberellin signaling pathway. Plant Signal Behav 15 (4), 1740872. https://coi.org/10.1080/15592324.2020.1740872.

Nelson, P.T., Goodman, M.M., 2008. Evaluation of elite exotic maize inbreds for use in temperate breeding. Crop Sci 48 (1), 85-92. https://coi.org/10.2135/cropsci2007.05.0287.\

Olsen, S.R., Cole, C.V., Watanabe, F.S., Dean, L.A., 1954. Estimation of available phosphorus in soils by extraction with sodium bicarbonate (939th ed.). Circular. U.S. Dept. of Agriculture Circular No. 939.

Pang, F., Li, Q., Solanki, M.K., Wang, Z., Xing, Y., Dong, D., 2024. Soil phosphorus transformation and plant uptake driven by phosphate-solubilizing microorganisms. Front Microbiol 15, 1383813. https://coi.org/10.3389/fmicb.2024.1383813.

Raymond, N. S., Gómez-Muñoz, B., van der Bom, F.J.T., Nybroe, O., Jensen, L.S., Müller-Stöver, D.S., Oberson, A., Richardson, A.E., 2021. Phosphate-solubilising microorganisms for improved crop productivity: a critical assessment. New Phytol 229 (3), 1268-1277. https://coi.org/10.1111/nph.16924.

Springer, N.M., Stupar, R.M., 2007. Allelic variation and heterosis in maize: how do two halves make more than a whole? Genome Res 17 (3), 264-275. https://coi.org/10.1101/gr.5347007.

Verbon, E.H., Liberman, L.M., 2016. Beneficial microbes affect endogenous mechanisms controlling root development. Trends Plant Sci 21 (3), 218-229. https://coi.org/10.1016/j.tplants.2016.01.013.

Peñuelas, J., Zheng, B., Tariq, A., Sardans, J., 2026. Microbial phosphorus cycling in terrestrial ecosystems. Nat. Rev. Microbiol 10-1038. https://coi.org/10.1038/s41579-026-01296-w.

VDLUFA. 1991. Die Untersuchung von Böden. 4th ed. VDLUFA-Verlag.Wagner, M.R., Roberts, J.H., Balint-Kurti, P., Holland, J.B., 2020. Heterosis of leaf and rhizosphere microbiomes in field-grown maize. New Phytol 228 (3), 1055-1069. https://coi.org/10.1111/nph.16730.

Wagner, M.R., Tang, C., Salvato, F., Clouse, K.M., Bartlett, A., Vintila, S., Phillips, L., Sermons, S., Hoffmann, M., Balint-Kurti, P.J., Kleiner, M., 2021. Microbe-dependent heterosis in maize. PNAS 118 (30). https://coi.org/10.1073/pnas.2021965118.

Wen, Z., Yu, P., Shen, J., Lambers, H., 2025. Do rhizosphere microbiomes match root functional traits? Trends Ecol. Evol 40 (9), 885-899. https://coi.org/10.1016/j.tree.2025.07.002.

Williams, A., Langridge, H., Straathof, A.L., Fox, G., Muhammadali, H., Hollywood, K.A., Xu, Y., Goodacre, R., de Vries, F.T., 2021. Comparing root exudate collection techniques: an improved hybrid method. Soil Biol Biochem 161, 108391. https://coi.org/10.1016/j.soilbio.2021.108391.

Xu, F., Liao, H., Yang, J., Zhang, Y., Yu, P., Cao, Y., Fang, J., Chen, S., Li, L., Sun, L., Du, C., Wang, K., Dang, X., Feng, Z., Cao, Y., Li, Y., Zhang, J., Xu, W., 2023. Auxin-producing bacteria promote barley rhizosheath formation. Nat Commun 14 (1), 5800. https://coi.org/10.1038/s41467-023-40916-4.

Xu, F., Wang, Y., Yang, J., Zhang, X., Wang, K., Ding, F., Pang, J., Tong, L., Bai, C., Chen, S., Sun, L., Du, C., Fang, J., Xu, M., Li, L., Yu, X., Gengli, J., Liu, J., Zhang, Q., Wang, Z., Zhu, Y., Zhang-Zheng, H., Zhang, J., Xu, W., 2025. Auxin-producing pseudomonas recruited by root flavonoids increases rice rhizosheath formation through the bacterial histidine kinase under soil drying. Adv. Sci 12 (34), e00607. https://coi.org/10.1002/advs.202500607.

Yang, J., Li, S., Zhou, X., Du, C., Fang, J., Li, X., Zhao, J., Ding, F., Wang, Y., Zhang, Q., Wang, Z., Liu, J., Dong, G., Zhang, J., Xu, F., Xu, W., 2025. Bacillus amyloliquefaciens promotes cluster root formation of white lupin under low phosphorus by mediating auxin levels. Plant Physiol 197 (2), kiae676. https://coi.org/10.1093/plphys/kiae676.

Ye, J., Liang, H., Zhao, X., Li, N., Song, D., Zhan, J., Liu, J., Wang, X., Tu, J., Varshney, R.K., Shi, J., Wang, H., 2023. A systematic dissection in oilseed rape provides insights into the genetic architecture and molecular mechanism of yield heterosis. Plant Biotechnol J 21 (7), 1479-1495. https://coi.org/10.1111/pbi.14054.

Yu, P., He, X., Baer, M., Beirinckx, S., Tian, T., Moya, Y.A.T., Zhang, X., Deichmann, M., Frey, F.P., Bresgen, V., Li, C., Razavi, B.S., Schaaf, G., von Wirén, N., Su, Z., Bucher, M., Tsuda, K., Goormachtig, S., Chen, X., Hochholdinger, F., 2021. Plant flavones enrich rhizosphere oxalobacteraceae to improve maize performance under nitrogen deprivation. Nat Plants 7 (4), 481-499. https://coi.org/10.1038/s41477-021-00897-y.

Zhan, J., Lin, L., Qiu, Y., Chen, S., Ji, W., Peng, Y., Yin, J., Guo, J., Xin, G., Fenton, O., Chen, H., 2026. Effect of soil organic phosphorus transformations on phosphorus availability during soil drying-wetting events: insights into abiotic and biotic processes. Soil Till Res 260, 107148. https://coi.org/10.1016/j.still.2026.107148.

Zhang, M., Wang, Y., Hu, Y., Wang, H., Liu, Y., Zhao, B., Zhang, J., Fang, R., Yan, Y., 2023. Heterosis in root microbiota inhibits growth of soil-borne fungal pathogens in hybrid rice.

J Integr Plant Biol 65 (4), 1059-1076. https://coi.org/10.1111/jipb.13416.
Zhao, B., Jia, X., Yu, N., Murray, J.D., Yi, K., Wang, E., 2024. Microbe-dependent and independent nitrogen and phosphate acquisition and regulation in plants. New Phytol 242 (4), 1507-1522. https://coi.org/10.1111/nph.19263.

Main figures

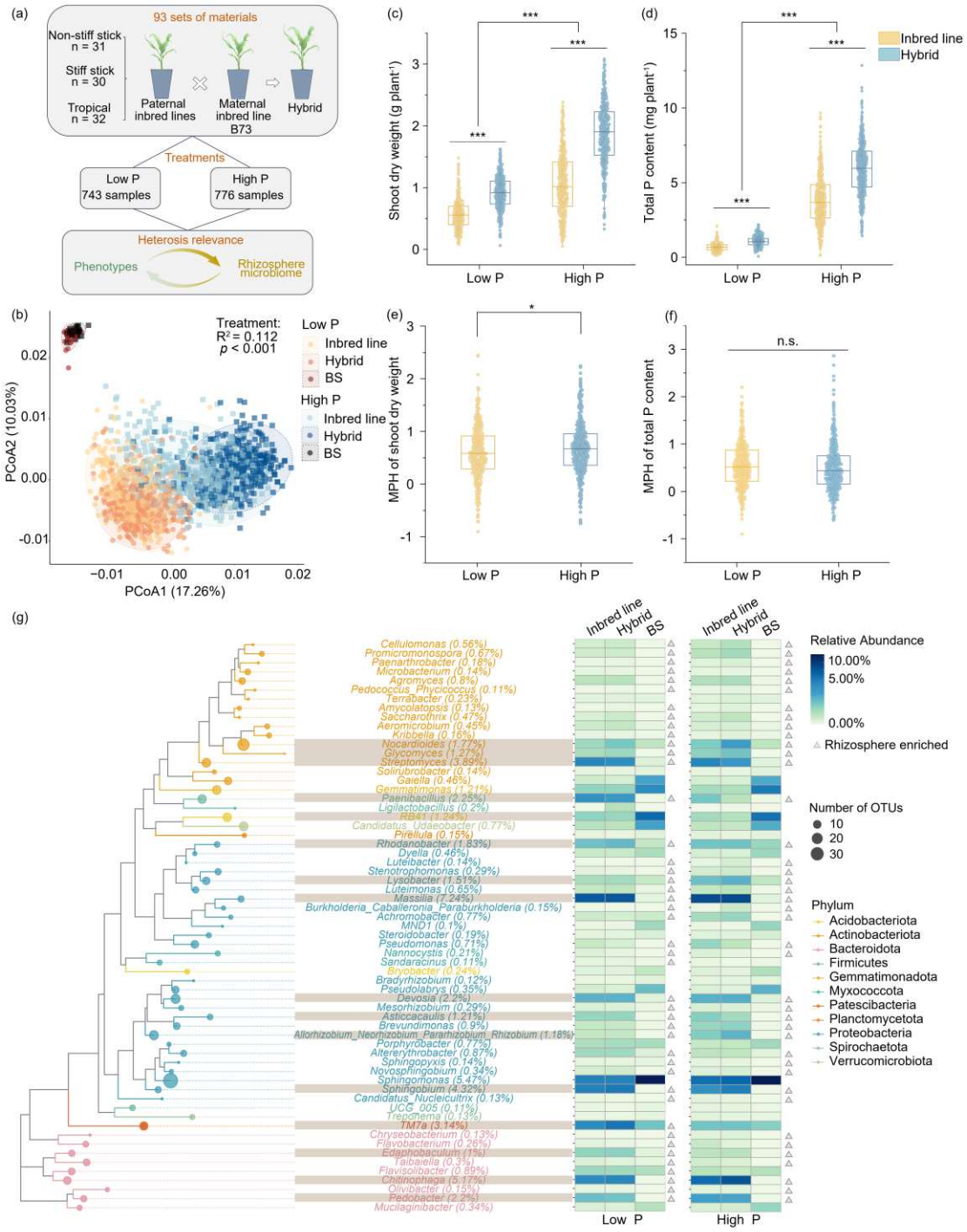


Fig. 1 Hybrid-specific rhizosphere microbiome assembly is associated with phosphorus acquisition in maize.

a, Experimental design and maize germplasm used in this study. A panel of 93 maize hybrid–inbred triplets was generated by crossing 93 paternal inbred lines representing three major heterotic groups (stiff stalk, non-stiff stalk, and tropical) with the common

maternal parent B73. Plants were grown under low-phosphorus (Low P) and high-phosphorus (High P) conditions. A total of 755 and 784 rhizosphere samples were collected under Low P and High P conditions, respectively.

b, Principal coordinate analysis (PCoA) of rhizosphere and bulk-soil bacterial communities based on Bray–Curtis dissimilarities at the ASV level. Statistical significance was assessed using PERMANOVA. "BS" denotes bulk soil, whereas "inbred line" and "hybrid" denote the corresponding rhizosphere samples; circles and squares represent Low P and High P condition, respectively.

c,d, Shoot dry biomass and shoot phosphorus accumulation of parental inbred lines and corresponding hybrids under Low P and High P conditions.

e,f, Mid-parent heterosis (MPH) for shoot dry biomass and shoot phosphorus accumulation under Low P and High P conditions.

For box plots (**c–f**), center lines indicate medians, box limits indicate the first and third quartiles, and whiskers represent the minimum and maximum values. Statistical significance was determined using two-sided Wilcoxon rank-sum tests ($P < 0.05$, $P < 0.01$, $P < 0.001$; n.s., not significant).

g, Phylogenetic distribution and relative abundance of dominant bacterial genera (mean relative abundance > 0.1%) across bulk soil, inbred-line rhizospheres, and hybrid rhizospheres under Low P and High P conditions. Circle sizes indicate the number of ASVs assigned to each genus. Genera are color-coded according to phylum-level taxonomy, and highly abundant genera (mean relative abundance > 1%) are highlighted. Heat maps show standardized mean relative abundance values for each bacterial genus. Hybrid-enriched taxa identified from these analyses were subsequently selected for functional characterization.

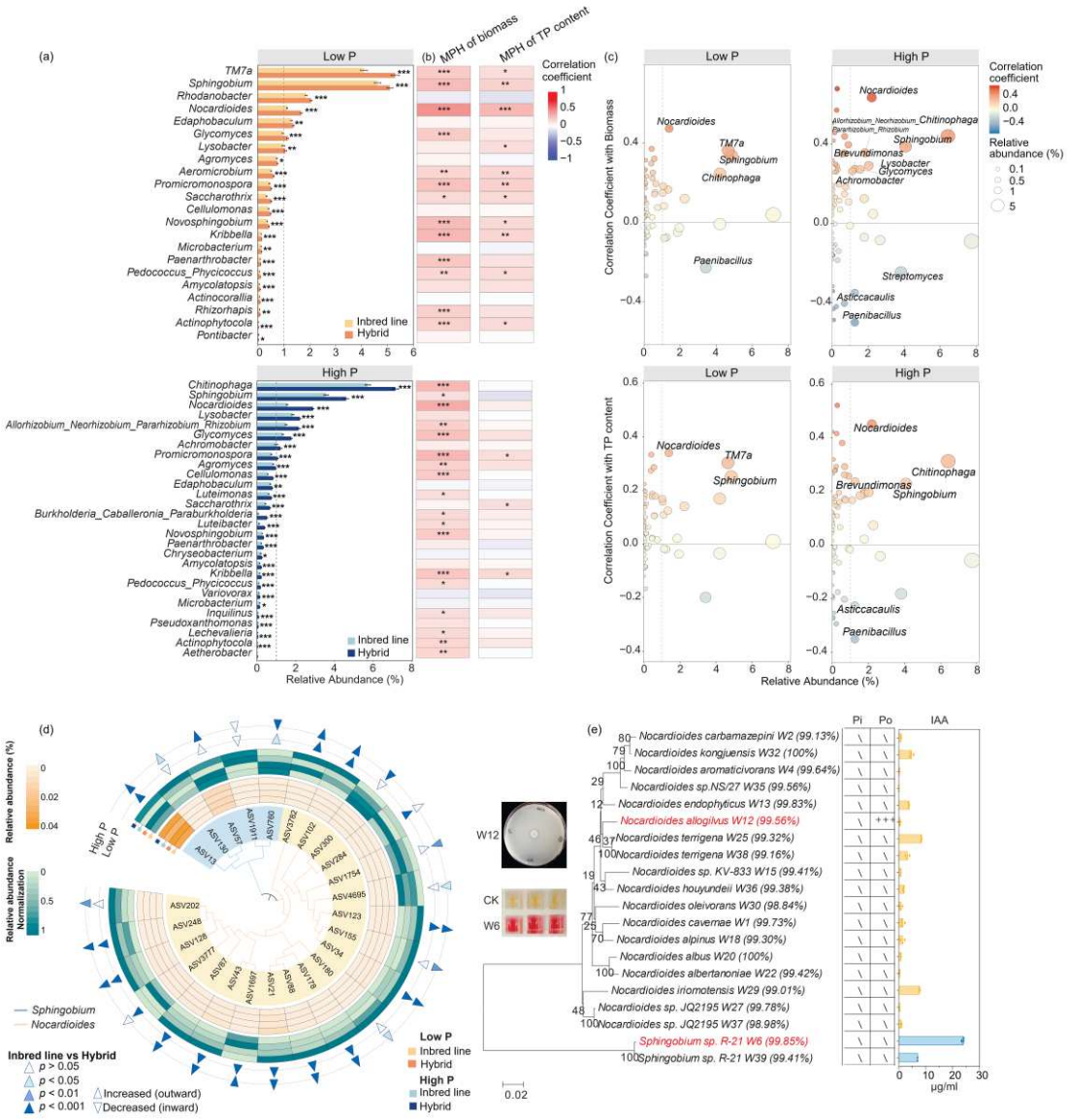


Fig. 2 Hybrid-enriched *Sphingobium* and *Nocardioides* exhibit distinct phosphorus-related functions.

a, Differentially abundant bacterial genera between hybrids and parental inbred lines under low-phosphorus (Low P) and high-phosphorus (High P) conditions. Bars indicate the difference in mean relative abundance between hybrids and inbred lines.

b, Heatmaps showing correlations between the mid-parent heterosis (MPH) of bacterial genera and the MPH of shoot biomass and shoot phosphorus accumulation under Low P and High P conditions.

c, Correlations between the relative abundance of dominant bacterial genera and plant phenotypes, including shoot biomass and shoot phosphorus accumulation. Circle size represents mean relative abundance, and circle color indicates Spearman's correlation coefficient. Only dominant genera (mean relative abundance ≥ 1%) with |r| > 0.2 and

FDR-adjusted $P < 0.05$ are shown.

d, Maximum-likelihood phylogeny of *Nocardioides* (23 ASVs; yellow) and *Sphingobium* (5 ASVs; blue) identified from 16S rRNA gene amplicon sequencing. The inner heat map shows ASV relative abundance, whereas the second heat map displays normalized abundance values under Low P and High P conditions. Outer triangles indicate differential abundance between hybrids and inbred lines under the respective phosphorus conditions. Outward-pointing triangles indicate enrichment in hybrids, whereas inward-pointing triangles indicate enrichment in inbred lines. Triangle shading reflects the statistical significance of abundance differences.

e, Neighbor-joining phylogeny of bacterial isolates obtained from maize roots grown under Low P conditions, including 18 *Nocardioides* isolates and 2 *Sphingobium* isolates. Functional characterization included inorganic phosphate (Pi) solubilization, organic phosphorus (Po) mineralization, and indole-3-acetic acid (IAA) production. IAA production values are shown as mean ± s.d. ($n = 3$ independent biological replicates).

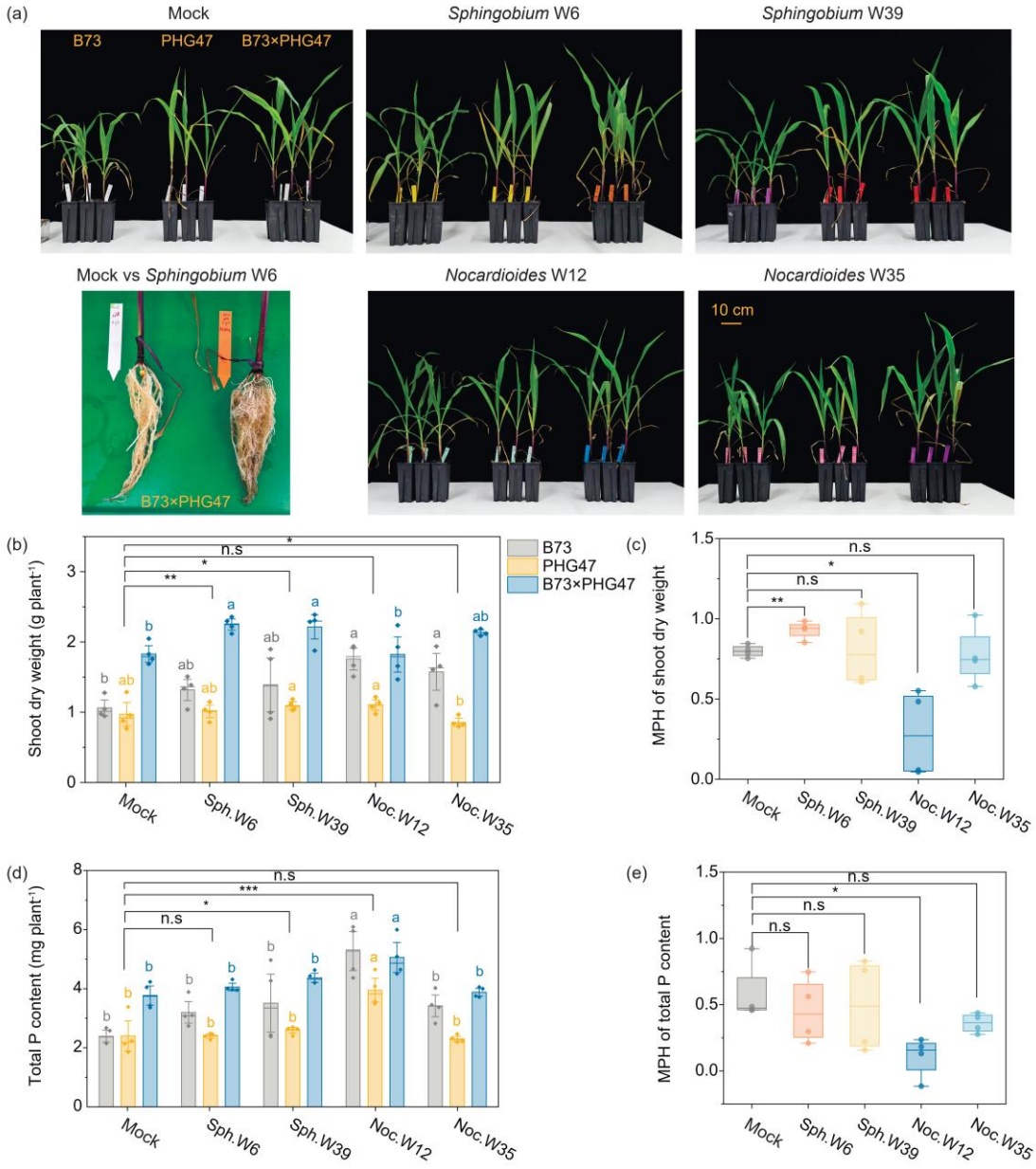


Fig. 3 Auxin-producing *Sphingobium* preferentially enhances maize heterosis under phosphorus deficiency.

a, Representative phenotypes of PHG47 (paternal inbred line), B73 (maternal inbred line), and their hybrid (B73 × PHG47) following inoculation with *Sphingobium* and *Nocardioides* strains under low-phosphorus (Low P) conditions. The inset shows representative root systems of hybrid plants inoculated with *Sphingobium* W6 or mock-treated controls.

b,d, Shoot dry biomass (**b**) and shoot phosphorus accumulation (**d**) of parental inbred lines and the corresponding hybrid following bacterial inoculation under Low P conditions.

c,e, Mid-parent heterosis (MPH) for shoot dry biomass (**c**) and shoot phosphorus accumulation (**e**) under different bacterial inoculation treatments.

For all box plots (**b-e**), center lines indicate medians, box limits indicate the first and third quartiles, and whiskers represent the minimum and maximum values (n = 4 independent biological replicates). Statistical significance between inoculation treatments was assessed using two-sided Wilcoxon rank-sum tests ($P < 0.05$, $P < 0.01$, $P < 0.001$; n.s., not significant). Different lowercase letters indicate significant differences among inoculation treatments within the same genotype, as determined by one-way ANOVA followed by Duncan's multiple range test ($P < 0.05$).

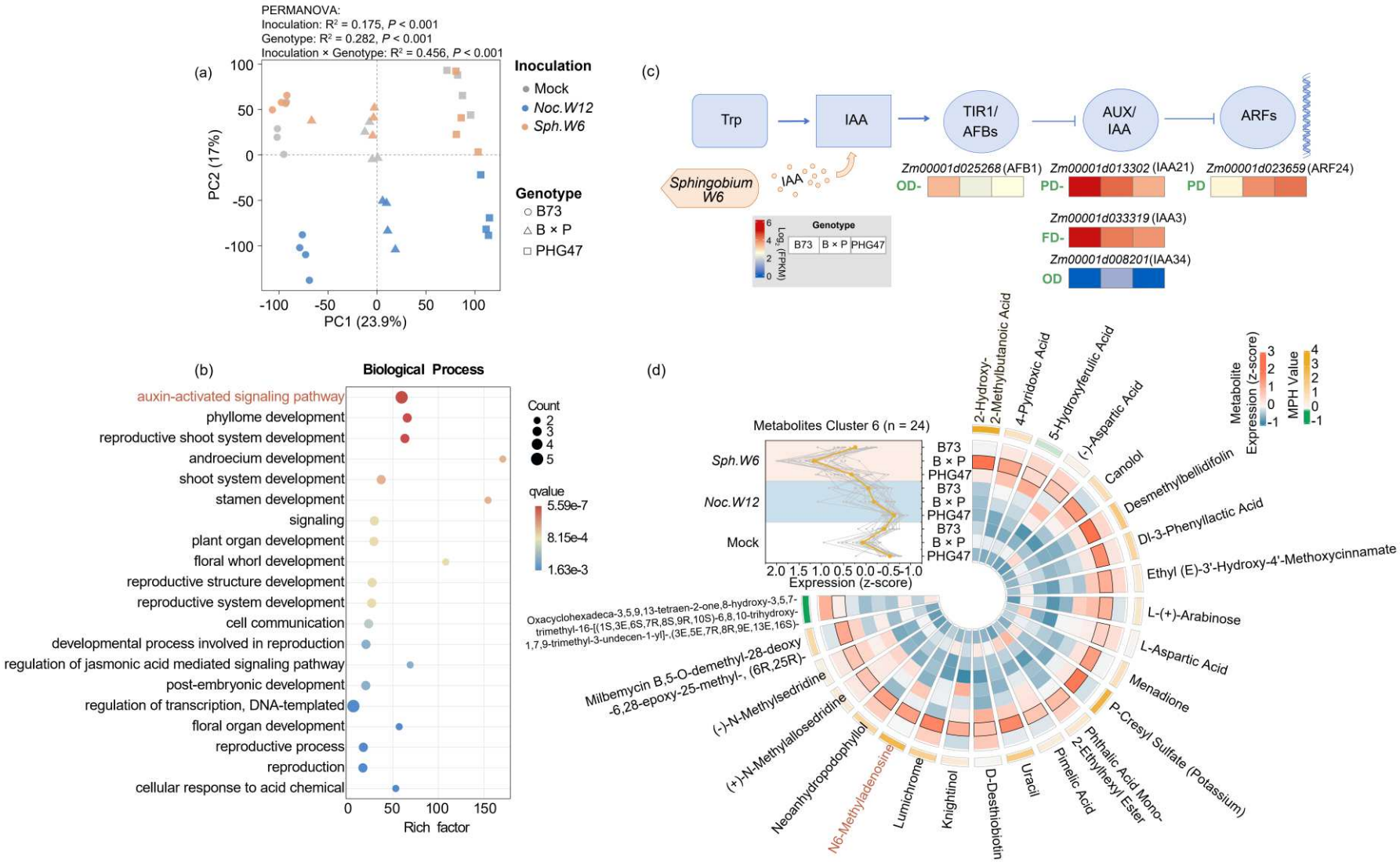

(a)
PERMANOVA:
Inoculation: R² = 0.175, P < 0.001
Genotype: R² = 0.282, P < 0.001
Inoculation × Genotype: R² = 0.456, P < 0.001
PC2 (17%)
PC1 (23.9%)
Inoculation
Mock
Noc.W12
Sph.W6
Genotype
B73
B × P
PHG47
(b)
Biological Process
auxin-activated signaling pathway
phyllome development
reproductive shoot system development
androecium development
shoot system development
stamen development
signaling
plant organ development
floral whorl development
reproductive structure development
reproductive system development
cell communication
developmental process involved in reproduction
regulation of jasmonic acid mediated signaling pathway
post-embryonic development
regulation of transcription, DNA-templated
floral organ development
reproductive process
reproduction
cellular response to acid chemical
Rich factor
Count
qvalue
5.59e-7
8.15e-4
1.63e-3
(c)
Trp
IAA
TIR1/ AFBs
AUX/ IAA
ARFs
Sphingobium W6
IAA
Zm00001d025268 (AFB1)
Zm00001d013302 (IAA21)
Zm00001d023659 (ARF24)
OD-
PD-
PD
Zm00001d033319 (IAA3)
FD-
Zm00001d008201(IAA34)
OD
Genotype
B73
B × P
PHG47
Log2 (FPKM)
(d)
Metabolites Cluster 6 (n = 24)
Sph.W6
Noc.W12
Mock
Expression (z-score)
Metabolite Expression (z-score)
MPH Value
2-Hydroxy-2-Methylbutanoic Acid
4-Pyridoxic Acid
5-Hydroxyferulic Acid
(-)-Aspartic Acid
Canolol
Desmethylbellidifolin
Dl-3-Phenyllactic Acid
Ethyl (E)-3'-Hydroxy-4'-Methoxycinnamate
L-(+)-Arabinose
L-Aspartic Acid
Menadione
P-Cresyl Sulfate (Potassium)
Phthalic Acid Mono-2-Ethylhexyl Ester
Pimelic Acid
Uracil
D-Desthiobiotin
Knightinol
Lumichrome
N6-Methyladenosine
Neoanhydropodophyllol
(+)-N-Methylallosedridine
(-)-N-Methylsedridine
Milbemycin B,5-O-demethyl-28-deoxy -6,28-epoxy-25-methyl-, (6R,25R)-
Oxacyclohexadeca-3,5,9,13-tetraen-2-one,8-hydroxy-3,5,7-trimethyl-16-[(1S,3E,6S,7R,8S,9R,10S)-6,8,10-trihydroxy-1,7,9-trimethyl-3-undecen-1-yl]-,(3E,5E,7R,8R,9E,13E,16S)-

Fig. 4 *Sphingobium* activates auxin-associated transcriptional and metabolic reprogramming in maize hybrids under phosphorus deficiency.

a, Principal component analysis (PCA) of root transcriptomes from PHG47 (paternal inbred line), B73 (maternal inbred line), and their hybrid (B73 × PHG47) under low-phosphorus (Low P) conditions following mock, *Sphingobium* W6, or *Nocardioides* W12 inoculation.

b, Functional enrichment analysis of non-additively expressed differentially expressed genes (NAE-DEGs) identified in the hybrid under *Sphingobium* W6 inoculation. Enriched Gene Ontology (GO) biological processes associated with plant hormone signaling are shown.

c, Expression patterns of NAE-DEGs involved in the auxin signaling pathway following *Sphingobium* W6 inoculation. Genes are grouped according to their dominance patterns. Color scale indicates normalized gene expression levels across genotypes.

d, Metabolite cluster specifically enriched in the hybrid following *Sphingobium* W6 inoculation, identified by k-means clustering analysis. The inner ring shows z-score-normalized metabolite abundance across treatments, whereas the outer ring represents the corresponding mid-parent heterosis (MPH) values of individual metabolites. Selected metabolites associated with hybrid-specific enrichment are highlighted.

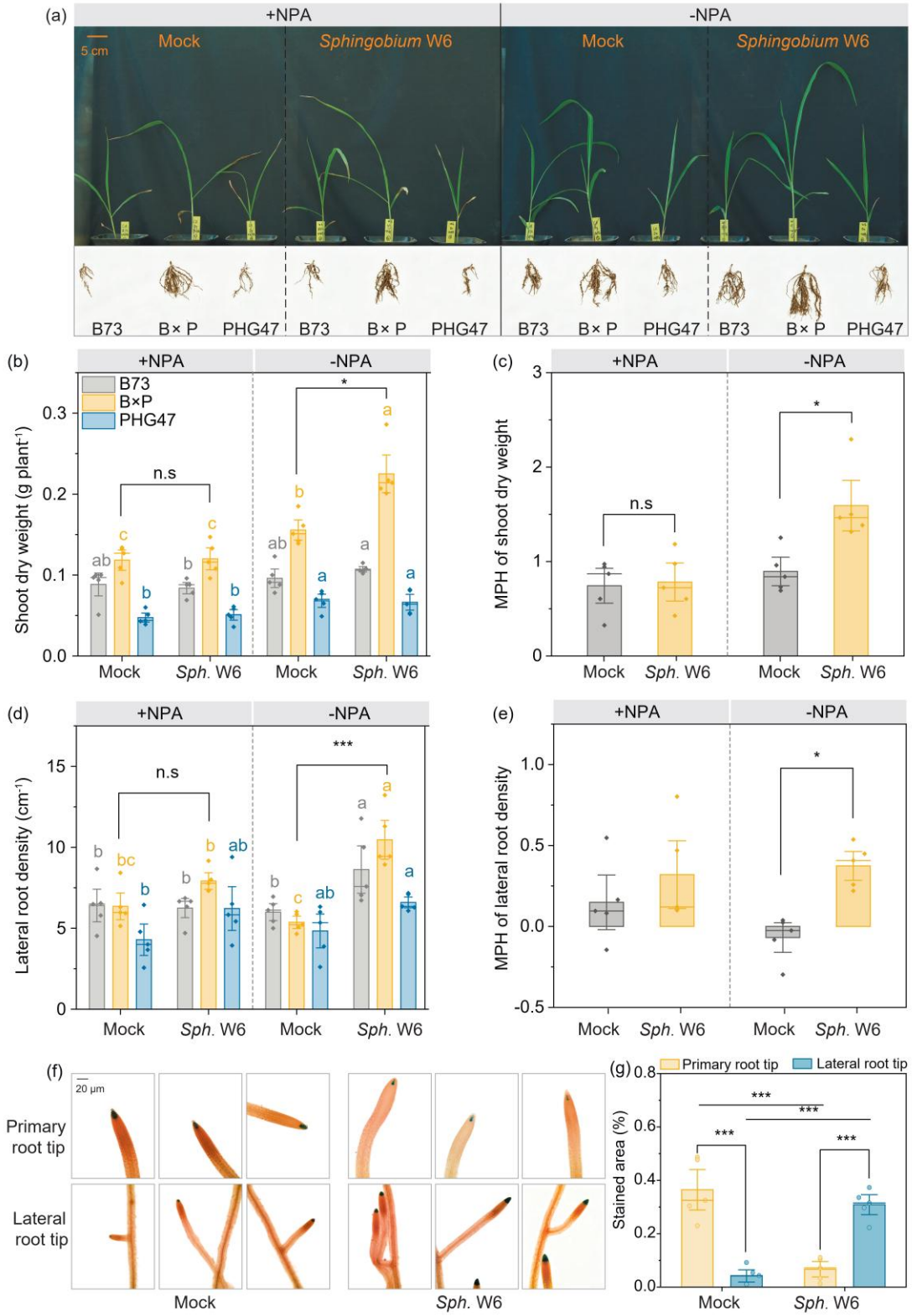


Fig. 5 *Sphingobium* promotes maize growth heterosis through host auxin signaling. **a,** Representative phenotypes of PHG47 (paternal inbred line), B73 (maternal inbred line), and their hybrid (B73 × PHG47) following *Sphingobium* W6 inoculation with or without application of the auxin efflux inhibitor N-1-naphthylphthalamic acid (NPA)

under low-phosphorus (Low P) conditions (n = 5 independent biological replicates per genotype).

b,d, Shoot dry biomass (**b**) and lateral root density (**d**) of the triplet under different combinations of *Sphingobium* W6 inoculation and NPA treatment under Low P conditions.

c,e, Mid-parent heterosis (MPH) for shoot dry biomass (**c**) and lateral root density (**e**) under different combinations of *Sphingobium* W6 inoculation and NPA treatment.

For box plots (**b-e**), center lines indicate medians, box limits indicate the first and third quartiles, and whiskers represent the minimum and maximum values. Statistical significance between treatments was assessed using two-sided Wilcoxon rank-sum tests ($P < 0.05$; n.s., not significant). Different lowercase letters indicate significant differences among treatments within the same genotype, as determined by one-way ANOVA followed by Duncan's multiple range test ($P < 0.05$).

f,g, (**f**) DR5::GUS reporter assay in *Arabidopsis thaliana* showing auxin-responsive activity in root tissues with or without *Sphingobium* W6 inoculation. Representative images illustrate altered spatial patterns of auxin accumulation in primary roots and lateral roots following bacterial inoculation. (**g**) GUS quantification of GUS-stained percentage in primary roots and lateral roots following bacterial inoculation. Statistical significance between inoculation treatments was assessed using two-sided Wilcoxon rank-sum tests ($P < 0.001$).

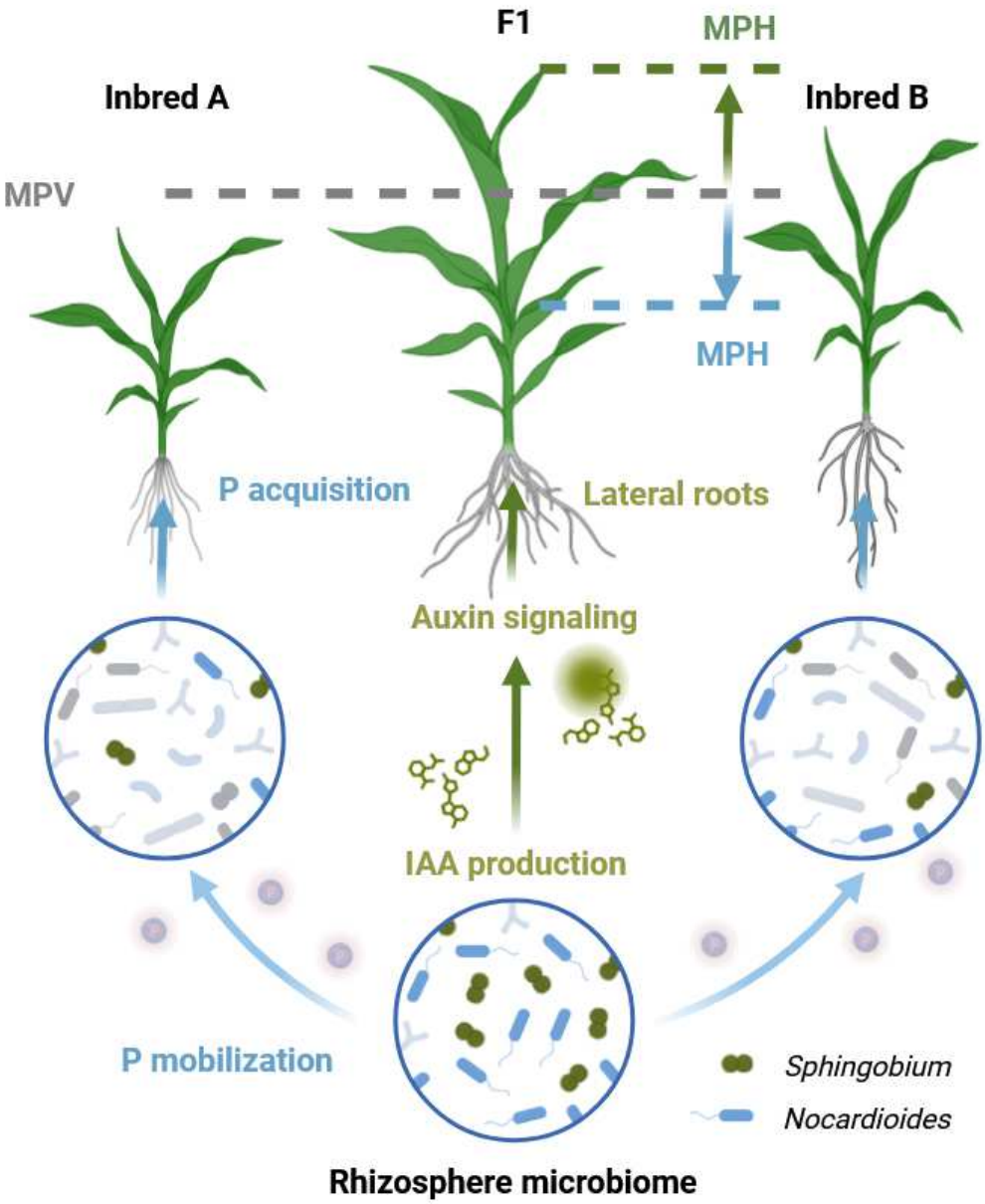


Fig. 6 Conceptual model of microbiome-mediated heterosis under phosphorus deficiency.

Phosphorus deficiency promotes hybrid-specific assembly of the rhizosphere microbiome. Maize hybrids preferentially enrich the auxin-producing bacterium *Sphingobium* W6, which stimulates host auxin signaling and lateral root development, thereby increasing root foraging capacity, phosphorus acquisition, and biomass heterosis. In contrast, phosphorus-mineralizing bacteria such as *Nocardioides* W12 improve phosphorus availability but contribute less to heterosis enhancement. The model suggests that microbial functions promoting root architectural plasticity may play a greater role in phosphorus-related heterosis than direct phosphorus mobilization. MPV, mid-parent value; MPH, mid-parent heterosis. P, phosphorus.

Supplementary Files

This is a list of supplementary files associated with this preprint. Click to download.

- Sourcedata.xlsx
- Supplementaryinformation.pdf